28. C. Arpigny, in *Elements and Isotopes in the Universe* (22nd Colloquium in Astrophysics, University of Liège, Liège, 1979), pp. 189–197.
29. D. Sears and R. T. Dodd, in *Meteorites and the Early Solar System*, J. F. Kerridge and M. S. Matthews, Eds. (Univ. of Arizona Press, Tucson, 1988), pp. 3–31. Rare exceptions consist of fine beads of pure Fe exsolved from olivines in chondrites during reheating in a reducing environment [see A. Kracher, E. R. D. Scott, K. Keil, *J. Geophys. Res.* **89**, B559 (1984)].
30. The complete loss of signal for oxygen in some spectra was reported as a peculiar feature of PUMA instruments by E. N. Evlanov *et al.*, in *Chemistry in Space*, J. M. Greenberg and V. Pirronello, Eds. (Kluwer Academic, Dordrecht, Netherlands, 1991), pp. 383–397.
31. J. F. Kerridge, A. L. Mackay, W. V. Boynton, *Science* **205**, 395 (1979).
32. M.N.F. and L.-A.M. thank California Space Institute and S. Ride for support during the completion of this work. This work was supported in part by National Aeronautics and Space Administration (NASA) grants. J.F.K. was supported through NASA grant NAGW 347. We thank D. E. Brownlee for his constructive comments as a referee.

4 February 1992; accepted 14 July 1992

X-ray Laser Microscopy of Rat Sperm Nuclei

L. B. Da Silva,* J. E. Trebes, R. Balhorn, S. Mrowka, E. Anderson, D. T. Attwood, T. W. Barbee, Jr., J. Brase, M. Corzett, J. Gray, J. A. Koch, C. Lee, D. Kern, R. A. London, B. J. MacGowan, D. L. Matthews, G. Stone

The development of high brightness and short pulse width (<200 picoseconds) x-ray lasers now offers biologists the possibility of high-resolution imaging of specimens in an aqueous environment without the blurring effects associated with natural motions and chemical erosion. As a step toward developing the capabilities of this type of x-ray microscopy, a tantalum x-ray laser at 44.83 angstrom wavelength was used together with an x-ray zone plate lens to image both unlabeled and selectively gold-labeled dried rat sperm nuclei. The observed images show ~500 angstrom features, illustrate the importance of x-ray microscopy in determining chemical composition, and provide information about the uniformity of sperm chromatin organization and the extent of sperm chromatin hydration.

Historically, advances in imaging technology have led to new and exciting results in the field of biology. Today, electron microscopy (EM), optical microscopy (OM), and atomic force microscopy (AFM) are necessary tools for biologists and biochemists around the world. These techniques offer high resolution (<20 Å for EM/AFM) of prepared specimens or lower resolution (~2000 Å for OM) of specimens in their natural environment. An alternative imaging technology that is now becoming available is x-ray microscopy, which offers the possibility of high-resolution imaging (~200 to 300 Å) of specimens in their natural environment. In addition, x-ray microscopy with the use of x-rays of different wavelengths can be used to probe the interior of living cells. This is currently practical only with OM.

To date, x-ray microscopy has been developed and demonstrated by several groups around the world. Resolutions near the diffraction limit have been reported by Jacobsen *et al.* (*1*) and Meyer-Ilse *et al.* (*2*); both groups used synchrotron radiation to image biological systems. X-rays generated in a laser-produced plasma were recently used by Tomie *et al.* (*3*) to produce 0.5-ns flash contact x-ray images of a hydrated sperm cell with a spatial resolution of ~1000 Å. Extending the use of laser plasma sources to imaging microscopy where chromatic aberrations necessitate the use of narrow bandpass optics will reduce signal levels. A narrow band 182 Å x-ray laser was previously used to produce contact x-ray micrographs of dry cervical cancer cells (*4*). However, only recently have x-ray lasers with wavelengths near and inside the water window (23 to 44 Å) been developed (*5*) that have sufficient output energy for microscopy of a wide range of biological objects. We recently demonstrated x-ray imaging using such an x-ray laser as the illuminator (*6*). The key advantage of an x-ray laser is that its high brightness and short duration allow images to be made with a single ~200-ps exposure. This eliminates the problems associated with motion blurring and radiation-induced chemical decomposition of the specimen. In addition, the quasi-monochromatic property of x-ray lasers makes them well suited to x-ray optics. In this report we discuss images taken of dried rat sperm nuclei with the use of this short-pulse x-ray laser source.

The x-ray imaging microscope we used is shown schematically in Fig. 1. X-rays from a nickel-like tantalum collisionally pumped x-ray laser (*7*) operating at 44.83 Å are collected and focused onto a specimen that is then imaged in transmission by a Fresnel zone plate lens (*8*) on a microchannel plate detector. The x-ray laser was generated by irradiation of a 3.5 cm long, 2000 Å thick plastic foil coated with 900 Å of tantalum with two cylindrically focused visible light (0.53 μm) laser beams. The heated foil explodes to form a high-temperature plasma with low-density gradients (*9*). For our experiment, two optical beams from the Nova Laser at Lawrence Livermore National Laboratory were used to generate an intensity on target of 3.0×10^{14} W/cm^2 for a duration of 500 ps (*7*). The x-ray laser originates from an ~100-μm-diameter gain region at the center of the plasma and has a beam divergence of 10 mrad [full width at half maximum (FWHM)]. The output energy is ~10 μJ in a 200-ps (FWHM) pulse that corresponds to a brightness of 10^{21} photons/(s mrad^2 mm^2 0.01% bandwidth). This is four orders of magnitude brighter than the X-1A beam line at the National Synchrotron Light Source, currently the world's brightest soft x-ray synchrotron beam line.

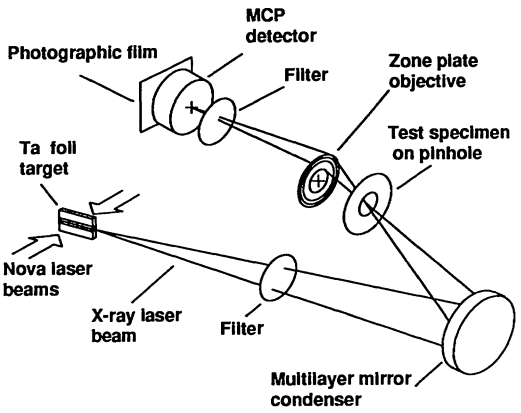

Fig. 1. Schematic of the x-ray microscope showing its main components. MCP, microchannel plate.

L. B. Da Silva, Department of Physics, University of California at Berkeley, Berkeley, CA 94720.
J. E. Trebes, R. Balhorn, S. Mrowka, T. W. Barbee, Jr., J. Brase, M. Corzett, J. A. Koch, C. Lee, R. A. London, B. J. MacGowan, D. L. Matthews, G. Stone, Lawrence Livermore National Laboratory, P.O. Box 808, Livermore, CA 94550.
E. Anderson and D. T. Attwood, Center for X-ray Optics, Lawrence Berkeley Laboratory, Berkeley, CA 94720.
J. Gray, Division of Molecular Cytometry, University of California at San Francisco, San Francisco, CA 94143.
D. Kern, IBM T. J. Watson Research Center, P.O. Box 218, Yorktown Heights, NY 10598.
*To whom correspondence should be addressed.

The x-ray laser beam is collected and focused on the object with a spherical x-ray mirror coated with tungsten-carbide/carbon multilayers (*10*). The mirror has a measured normal incidence reflectivity of 5% and a bandpass of 1.5% at the x-ray laser wavelength of 44.83 Å. The narrow bandpass of the mirror serves to eliminate most of the background soft x-ray continuum produced in the gain region. The mirror has a radius of curvature of 1 m and is operated slightly off axis at an angle of 1.4 degrees. The laser-to-mirror distance is 3.0 m, which isolates the sample from the laser-produced plasma and results in a ×5 demagnification of the x-ray laser source region. A 10-mrad aperture limits the section of the mirror used to a 3-cm-diameter region centered on the optic. A filter (2000 Å titanium on 2000 Å of Lexan) placed between the mirror and the x-ray laser further protects the sample by eliminating scattered optical radiation. The zone plate we used has 500 zones, an outer radius of 45 μm, an outer zone width of 450 Å, and a focal length of 900 μm at 44.83 Å. The Rayleigh resolution of the zone plate lens is calculated to be ~550 Å.

Using this x-ray microscope, we began to study how DNA is organized inside the mammalian sperm cell. The sperm is unique in that the DNA is packaged inside the nucleus by a small protein, called protamine, in a highly compacted state. Transmission electron microscopy studies have shown the fibers of DNA and protamine to be so tightly packed inside the nucleus of the mature sperm that internal features of structure cannot be resolved (*11*). Studies of the surface by AFM (*12*) have indicated that the DNA is packaged in 600 to 1000 Å nodules. EM images of freeze-fractured sperm heads by Koehler and co-workers (*13, 14*) have also suggested that the DNA is further organized into 8 to 12 sheet-like subdomains called lamellae.

We prepared three different types of rat sperm nuclei by treating sperm isolated from rat epididymides with a disulfide reducing agent and detergent (*15*) to dissolve the tails, acrosome, and nuclear membranes, exposing the DNA-protamine complex that comprises sperm chromatin. A droplet containing the amembranous nuclei was deposited on a silicon nitride window (300 by 300 μm, 1000 Å thick), and the liquid containing unbound nuclei was removed after 30 s. The window was washed three times in distilled water and air-dried before imaging.

The positions of particular nuclei were located on the window by light microscopy, and these nuclei were imaged with both the x-ray microscope and the AFM. The x-ray image of an amembranous rat sperm nucleus prepared by this method (Fig. 2A) shows very little internal structure, which indicates

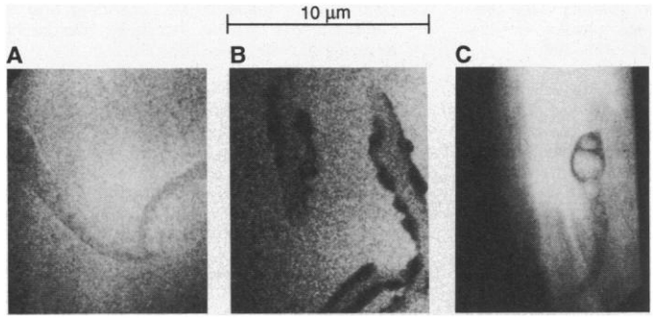

Fig. 2. X-ray microscope images of rat sperm nuclei (**A**) with no gold labeling, (**B**) stained with antiprotamine 1 and gold-labeled, and (**C**) stained with antiprotamine 2 and gold-labeled.

a very uniform packing density over ~500 Å scale lengths. AFM images of the same nucleus indicate that its thickness varies from 4500 to 8000 Å. In a region that measures 7000 Å by AFM, the x-ray laser images show approximately 60 ± 5% transmission at the x-ray wavelength of 44.83 Å. Using the composition of the protamine-DNA complex (*16*) and a density of 1.6, we calculated the thickness from the x-ray transmission data to be 4700 Å, significantly less than that observed by AFM. This difference (2300 Å) appears to relate to the presence of considerable amounts of tightly bound water within the complex. This water, for all practical purposes, would appear transparent to the x-rays.

These results are consistent with recent AFM studies of mouse and bull sperm, which show that ~58 to 72% of the volume of the sperm nucleus is occupied by water (*17*). The majority of this water is lost upon dehydration in air. Our x-ray microscopy results suggest that as much as one-third of the amembranous nuclear volume may be contributed by water that is retained by the chromatin even after 20 min at reduced pressure (10^{-5} torr). Clearly, this value must represent an upper limit. Whereas the chromatin must contain some additional proteins (a minor component of histone and small amounts of nuclear matrix or other proteins), this protein represents only a very small component relative to protamine and the water of hydration.

We have also obtained images of rat sperm chromatin stained with mouse antibodies to protamine 1 and protamine 2 (antiprotamine 1 and antiprotamine 2, respectively) and goat antimouse antibodies tagged with 400 Å diameter gold. Images of two of these stained rat sperm (Fig. 2, B and C) show distinct differences. Although both images show high concentrations of gold along the edge of the sperm and some evidence of individual 400 Å gold particles on the surface, the clumping of the gold labels is particularly evident in the image of the nuclei stained with the antiprotamine 1 (Fig. 2B). Although the mouse primary antibody is present in sufficient concentration to coat the surface of the rat sperm nucleus

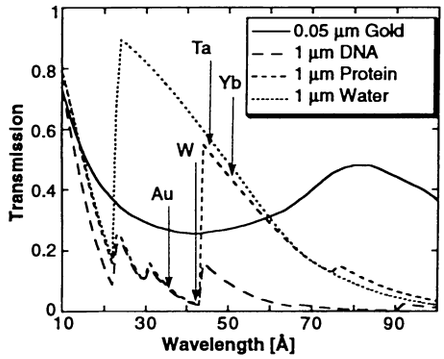

Fig. 3. X-ray transmission through 1 μm of DNA, protein ($C_{52}H_7O_{22}N_{16}S$, r = 1.35 g/cm^2), and water and 0.05 μm of gold. The wavelengths of demonstrated nickel-like x-ray lasers are indicated by arrows and the corresponding element. By taking advantage of the sharp absorption edges and available x-ray lasers, one can map out element abundance.

in these samples, the gold-labeled secondary antibody is not. Consequently, only partial staining of the surface with the gold-tagged secondary antibody was achieved. This allowed us to resolve large clumps of gold as well as individual particles.

The structures observed in the antiprotamine 2–stained nuclei (Fig. 2C) appear to result from the limited labeling of disrupted sperm nuclei with gold. Analysis of the digitized images indicates that the internal wall-like structure is very sharp with a 10 to 90% rise in intensity over 500 Å. The unusual staining patterns observed in Fig. 2C were observed only when the antiprotamine 2–stained sperm nuclei were purified by sedimentation through 30% glycerol. Many of these nuclei were partially decondensed as a result of exposure to glycerol, generating vacuoles within the nucleus and unmasking internal sites for antibody binding that are not normally accessible to antibody. Sperm nuclei stained with antiprotamine 2 and washed by sedimentation through buffer without glycerol remained intact and contained only a few isolated gold particles attached to the edges of the nucleus.

In addition to providing new information about the hydration state of sperm

chromatin, these x-ray images of rat sperm nuclei have also demonstrated that x-ray lasers can resolve structures as small as 500 Å attached to biological structures. Whereas additional studies must be performed to refine the estimates of tightly bound water in sperm chromatin provided by these images, these results support recent AFM studies that show that sperm chromatin must be extensively hydrated. This water of hydration, which may contribute as much as one-third of the volume of the rat sperm nucleus, is most likely located within the 600 to 1000 Å nodules of sperm chromatin (*12*) and between lamellae (*13*, *14*).

An advantage of x-ray microscopy that will prove useful in future studies is that it can also be used to obtain information about elemental density. By selecting an appropriate x-ray laser wavelength, one can enhance the contrast between elements. In Fig. 3, we show the wavelengths of demonstrated nickel-like x-ray lasers along with the calculated transmission for 1 μm of water, DNA, and protein and for 500 Å of gold. The large change in absorption across the carbon absorption edge at 44.3 Å can be used to map out carbon abundance when two images of the specimen are taken, one with the tantalum x-ray laser (44.83 Å wavelength) and one with the tungsten x-ray laser (43.8 Å wavelength). Such data obtained for rat sperm nuclei, for example, would provide the additional information we need to better estimate the extent of sperm chromatin hydration.

The 44.83 Å wavelength of the nickel-like tantalum x-ray laser used in these experiments is nearly optimal for the imaging of biological specimens that have been immunogold-labeled. The development of normal incidence multilayer x-ray optics at wavelengths below the carbon K-edge (43.7 Å), where there is high contrast between proteins and water, will make short wavelength x-ray laser microscopes possible. Theoretical calculations indicate that short wavelength x-ray optics can be fabricated with existing technology, and we expect several groups to succeed within a year. In addition, improvements in the capability of current x-ray lasers through the use of multilayer mirrors to double-pass the gain region or through increasing the laser gain should lead to 100 to 1000 times more output. The increase in energy will allow combining several microscopes to produce images of the object along different lines of sight. These multiple frames could be synchronized to obtain three-dimensional images or time-delayed to observe the effects of high dosage on specimens. In addition, new glass laser technology affording high average power should allow the construction of x-ray lasers that are more compact (3 by 10 m) than the Nova laser and cost less ($1 million rather than several hundred million dollars) and that offer reasonable repetition rates (once every 5 to 10 min) (*18*).

REFERENCES AND NOTES

1. C. Jacobsen *et al.*, *Opt. Commun.* **86**, 351 (1991).
2. W. Meyer-Ilse *et al.*, in *X-Ray Microscopy III*, A. Michette, G. Morrison, C. Buckley, Eds. (Springer-Verlag, Berlin, 1991), pp. 284–289.
3. T. Tomie *et al.*, *Science* **252**, 691 (1991).
4. C. H. Skinner *et al.*, *J. Microsc.* **159**, 51 (1990).
5. B. J. MacGowan *et al.*, in *X-Ray Lasers 1990*, G. J. Tallents, Ed. (IOP Publishing, York, United Kingdom, 1990), pp. 221–230.
6. L. B. DaSilva *et al.*, *Opt. Lett.* **17**, 754 (1992).
7. B. J. MacGowan *et al.*, *Phys. Rev. Lett.* **65**, 420 (1990).
8. E. Anderson and D. Kern, in *X-Ray Microscopy III*, A. Michette, G. Morrison, C. Buckley, Eds. (Springer-Verlag, Berlin, 1991), pp. 75–78.
9. M. D. Rosen *et al.*, *Phys. Rev. Lett.* **54**, 106 (1985).
10. T. W. Barbee, *Opt. Eng.* **29**, 581 (1990).
11. G. B. Dooher and D. Bennett, *Am. J. Anat.* **136**, 339 (1973).
12. M. J. Allen, G. C. Pogany, W. Siekhaus, R. Balhorn, *J. Cell Biol.* **111**, 110 (1990).
13. J. K. Koehler, *J. Ultrastruct. Res.* **33**, 598 (1970).
14. J. Koehler, U. Wurschmidt, M. P. Larsen, *Gamete Res.* **8**, 357 (1983).
15. R. Balhorn, B. L. Gledhill, A. Wyrobek, *Biochemistry* **16**, 4704 (1977).
16. The protamine-DNA complex consists of 1 molecule of protamine to 10 bp of DNA and is designated by the formula $C_{477}H_{757}O_{179}N_{214}P_{20}S_9$.
17. M. J. Allen *et al.*, *J. Cell Biol.* **115**, 50 (1991).
18. J. T. Hunt, in *Solid State Lasers II*, G. Dube, Ed. [Society of Photo-Optical Instrumentation Engineers (SPIE) proceedings, Los Angeles, 1991], vol. 1410, pp. 2–14.

19. The authors are indebted to J. Kilkenny, M. Eckart, R. Stewart, and the Nova Experiments Group for support and assistance. We would also like to thank J. Cox, R. Wing, M. Carter, R. Levesque, F. Kelly, D. Montgomery, and G. Shimkaveg for their contributions. Supported by U.S. Department of Energy Office of Health and Environmental Research and performed under the auspices of the U.S. Department of Energy by the Lawrence Livermore National Laboratory under contract W-7405-ENG-48. The work at the Lawrence Berkeley Laboratory is supported by the U.S. Department of Energy Office of Basic Energy Sciences and the Air Force Office of Scientific Research.

12 June 1992; accepted 13 August 1992

Room-Temperature, Electric Field–Induced Creation of Stable Devices in $CuInSe_2$ Crystals

David Cahen,* Jean-Marc Gilet, Claus Schmitz,† Leonid Chernyak, Konstantin Gartsman, Abram Jakubowicz‡

Multiple-junction structures were formed, on a microscopic scale, at room temperature, by the application of a strong electric field across originally homogeneous crystals of the ternary chalcopyrite semiconductor $CuInSe_2$. After removal of the electric field, the structures were examined with electron beam–induced current microscopy and their current-voltage characteristics were measured. Bipolar transistor action was observed, indicating that sharp bulk junctions can form in this way at low ambient temperatures. The devices are stable under normal (low-voltage) operating conditions. Possible causes for this effect, including electromigration and electric field–assisted defect reactions, are suggested.

The use of semiconductors in devices depends critically on our ability to tailor their electronic properties. This is achieved chemically by doping, which is the controlled introduction of species different from those making up the semiconductor. The dopants are usually foreign species and they are introduced by thermal diffusion or ion implantation. Both are high-energy processes. We have found that controlled, local changes in the concentrations of dopants can be made, at ambient temperature, in ternary chalcogenide semiconductors, especially $CuInSe_2$, without the introduction of any foreign species, as a result of the action of strong electric fields (*E* fields). The process is illustrated by the formation of bipolar transistor structures.

The use of *E* fields to change preexisting doping profiles obtained by thermal diffusion goes back to the early days of Si and Ge semiconductor science (*1*, *2*). Indeed, the compensated material needed for the action of Si:Li detectors is obtained by controlled electromigration of Li after its thermal indiffusion into Si (*3*). The so-called "forming" of contacts to Se rectifiers has also been related to dopant electromigration (*4*). Other examples of the action of *E* fields on semiconductor doping include deep-level defect gettering in Si, Ge, or GaAs (*5*–*7*).

The relative ease by which $CuInSe_2$ (CISe) can be doped to yield *n*- or *p*-type CISe has been ascribed to its doping by native defects (*8*) (although doping by foreign species is possible as well). Thus diodes have been formed in originally *p*-CISe by thermal indiffusion of Cu or In (*9*, *10*); facile homojunction formation was observed in single-crystal CISe as a result of

Department of Materials and Interfaces, Weizmann Institute of Science, Rehovot, Israel.

*To whom correspondence should be addressed.
†Present address: Institut für SOLARE Energieversorgungstechnik, Kassel, Germany.
‡Present address: IBM Research Laboratories, Rüschlikon, Switzerland.